The Company of **Biologists**

RESEARCH ARTICLE

BMP signalling controls the construction of vertebrate mucociliary epithelia

Marie Cibois[1,‡], Guillaume Luxardi[1,*,‡], Benoit Chevalier[2,‡], Virginie Thomé[1], Olivier Mercey[2,3], Laure-Emmanuelle Zaragosi[2,3], Pascal Barby[2], Andrea Pasini[1,§], Brice Marcet[2,3,§] and Laurent Kodjabachian[1,§,¶]

ABSTRACT

Despite the importance of mucociliary epithelia in animal physiology, the mechanisms controlling their establishment are poorly understood. Using the developing *Xenopus* epidermis and regenerating human upper airways, we reveal the importance of BMP signalling for the construction of vertebrate mucociliary epithelia. In *Xenopus*, attenuation of BMP activity is necessary for the specification of multiciliated cells (MCCs), ionocytes and small secretory cells (SSCs). Conversely, BMP activity is required for the proper differentiation of goblet cells. Our data suggest that the BMP and Notch pathways interact to control fate choices in the developing epidermis. Unexpectedly, BMP activity is also necessary for the insertion of MCCs, ionocytes and SSCs into the surface epithelium. In human, BMP inhibition also strongly stimulates the formation of MCCs in normal and pathological (cystic fibrosis) airway samples, whereas BMP overactivation has the opposite effect. This work identifies the BMP pathway as a key regulator of vertebrate mucociliary epithelium differentiation and morphogenesis.

KEY WORDS: *Xenopus*, Human, Mucociliary epithelium, Multiciliogenesis, BMP, Notch, Epidermis, Airway

INTRODUCTION

Mucociliary epithelia (MCE) are encountered in many bilaterians, where they perform a variety of functions, including animal movement, food particle capture and ingestion, gamete transportation, and protection against pollutants and infectious agents (Castillo-Briceno and Kodjabachian, 2014; Lyons et al., 2006; Rompolas et al., 2013; Silverman et al., 1999; Werner and Mitchell, 2012). One of the most widely studied MCE is the lining of the human upper airways, which ensures the clearance of inhaled noxious particles by means of the mucociliary escalator. Several chronic respiratory diseases, including asthma, chronic obstructive pulmonary diseases and cystic fibrosis, are associated with defects in MCE regeneration and impaired airway cleansing (Fahy and Dickey, 2010; Livraghi and Randell, 2007). More recently, familial cases of deficient mucociliary clearance have been linked to mutations in genes required for multiciliogenesis (Boon et al., 2014; Wallmeier et al., 2014). MCE are characterised by the presence of at least two cell types: mucus-secreting (goblet) cells and multiciliated cells (MCCs) with motile cilia that distribute and mobilise the mucus along the epithelial surface. The mammalian airway MCE also contains basally located cells that have stem cell-like features and are responsible for renewal and maintenance of the tissue (Hajj et al., 2007; Hogan et al., 2014; Rock et al., 2009). The cellular and molecular events controlling human airway MCE formation and renewal are incompletely understood, largely owing to the poor accessibility and experimental amenability of this tissue. Air-liquid interface (ALI) primary cultures of human airway epithelial cells (HAECs) from healthy or diseased donors provide a valuable tool to investigate these processes (Karp et al., 2002; Marcet et al., 2011), but are technically demanding and might not fully recapitulate the relevant interactions occurring within the organism.

Recent studies have suggested that the embryonic epidermis of the amphibian *Xenopus* might provide a powerful and valuable model to address vertebrate MCE biology (Cibois et al., 2014; Dubaissi and Papalopulu, 2011; Werner and Mitchell, 2012). In particular, several reports revealed a striking degree of conservation in the molecular mechanisms that control MCC differentiation in mammalian upper airways and in the *Xenopus* embryonic epidermis (Marcet et al., 2011; Song et al., 2014; Stubbs et al., 2012; Tan et al., 2013; Werner and Mitchell, 2012).

In its mature form, the *Xenopus* embryonic epidermis consists of an epithelial outer layer of goblet cells that is interspersed with MCCs, osmoregulatory ionocytes and serotonin-secreting small secretory cells (SSCs), and an inner layer of non-cohesive P63-positive cells (Deblandre et al., 1999; Dubaissi et al., 2014; Lu et al., 2001; Quigley et al., 2011; Walentek et al., 2014). This tissue emerges from the early non-neural ectoderm in a multistep process. During gastrulation, MCCs, ionocytes, SSCs and P63-positive cells are born within the inner layer. It has been reported that the Delta/Notch pathway controls the number of cells of each type, presumably via lateral inhibition. In this process, a so-called signal-sending cell displays ligand molecules, such as Delta, at its surface and transactivates Notch receptor molecules on the surface of adjacent signal-receiving cells, which allows the two cells to adopt distinct fates (Guruharsha et al., 2012). In the *Xenopus* epidermis, constitutive activation of Notch resulted in a decrease in the number of both MCCs and ionocytes, whereas blocking the Notch pathway led to an increase in their numbers (Deblandre et al., 1999; Hayes et al., 2007; Marcet et al., 2011; Quigley et al., 2011; Stubbs et al., 2006, 2012). However, there is evidence that *Xenopus* epidermal cells are sensitive to cis-inhibition of Notch by its ligands (Guruharsha et al., 2012), as Delta-like 1 (Dll1) overexpression induces supernumerary MCCs, similar to overexpression of the secreted dominant-negative Dll1[Stu] mutant (Deblandre et al., 1999). Finally, Notch activation was shown to induce supernumerary P63-positive cells, whereas Notch inhibition had the opposite effect, suggesting that P63-positive cells are counterparts to MCCs and ionocytes selected through lateral inhibition (Sirour et al., 2011). Following their commitment,
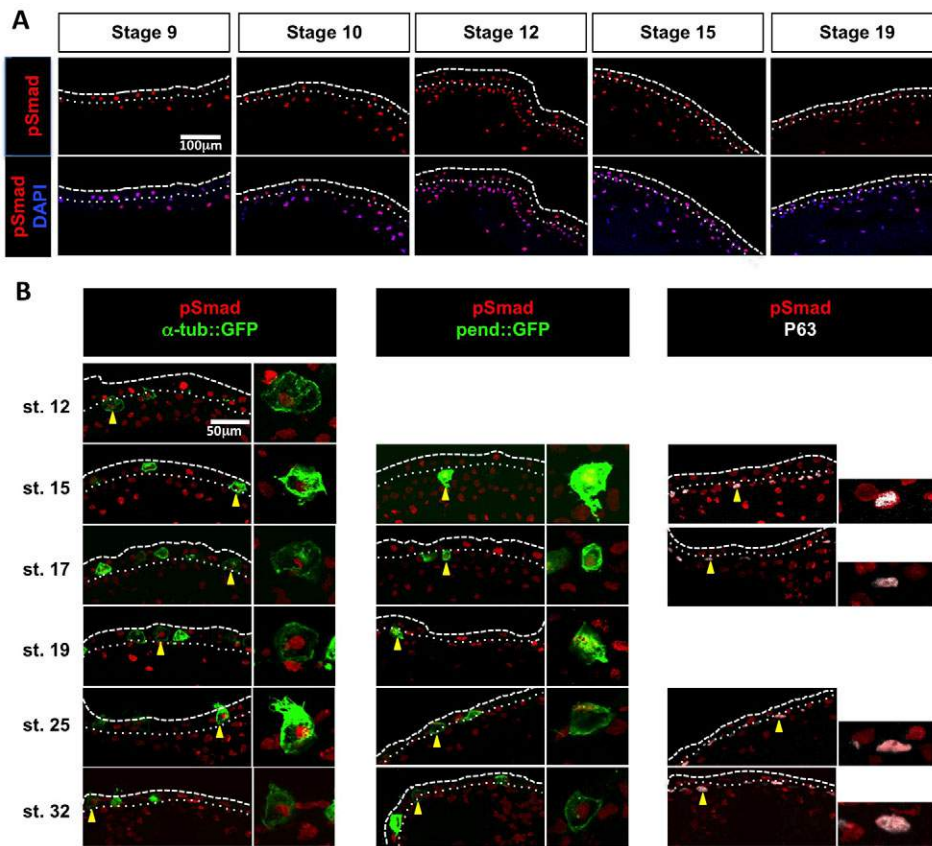
DEVELOPMENT

Fig. 1. BMP pathway activity in the developing *Xenopus* epidermis. (A) Immunostaining of cryosectioned *Xenopus* embryos revealed that the pSmad1/5/8 signal (red) colocalises with nuclear DAPI staining (blue) in both inner and outer layer cells. (B) (Left) In embryos injected with linearised plasmid DNA for the MCC reporter α-tub::GFP (50 pg/embryo), the pSmad1/5/8 signal (red) colocalised with GFP immunostaining (green). (Middle) In embryos injected with linearised plasmid DNA for the ionocyte reporter pendrin::GFP (25 pg/embryo), the pSmad1/5/8 signal (red) colocalised with GFP immunostaining (green). (Right) The pSmad1/5/8 signal (red) colocalised with P63 protein expression (white). For each marker and stage, a representative cell (yellow arrowhead) is displayed at higher magnification to show the double staining. The white dashed and dotted lines respectively mark the apical surface of the ectodermal outer layer and the boundary between the outer and the inner ectodermal layers.

MCCs, ionocytes and SSCs sequentially migrate to the outer layer, where they intercalate among goblet cells and resume differentiation (Chung et al., 2014; Cibois et al., 2014; Quigley et al., 2011; Stubbs et al., 2006), whereas the P63-positive cells remain in the inner layer. The role of P63-positive cells remains uncharacterised, although the mature inner layer of the amphibian embryonic epidermis has been proposed to constitute the source of the late larval and post-metamorphic skin (Yoshizato, 2007). Thus, *Xenopus* epidermal P63-positive cells may not be compared to the P63-positive bona fide basal stem cells of mammalian airway epithelia (Hogan et al., 2014).

In *Xenopus*, BMP signalling is chiefly responsible for non-neural ectoderm induction at blastula/gastrula stages (Cibois et al., 2014; De Robertis and Kuroda, 2004). Although BMP expression and activity remain high at subsequent stages (Schohl and Fagotto, 2002), the role of this pathway in the developing epidermis has never been addressed. In mammals, activation of the BMP pathway has been described in lung morphogenesis and homeostasis as well as in airway epithelium regeneration (Huang et al., 2014; Masterson et al., 2011; McCormack et al., 2013; Sountoulidis et al., 2012).

We show here that correct organogenesis of the *Xenopus* embryonic epidermis requires the fine-tuning of BMP signalling activity. BMP inhibition is necessary and sufficient to induce MCC, ionocyte and SSC specification, whereas correct goblet cell differentiation depends on high BMP activity. BMP activity is also required for the insertion of MCCs, ionocytes and SSCs into the outer layer. Furthermore, in HAECs from healthy donors and from cystic fibrosis patients, BMP pathway inhibition stimulates MCE differentiation, with a dramatic increase in MCC numbers, whereas treatment with recombinant BMPs globally blocks cell differentiation.

Altogether, our data highlight the importance of the BMP pathway in the construction of vertebrate MCE.

RESULTS

The BMP pathway is active during MCE development and regeneration

Phosphorylation of Smad1/5/8 (pSmad1/5/8), which indicates BMP activity, was detected in the nuclei of most non-neural ectoderm cells in *Xenopus*, in both the outer and inner ectodermal layers and at all stages analysed, ranging from blastula to tailbud (Fig. 1A). To map the cell populations that receive BMP signals in the inner layer, we performed pSmad1/5/8 immunodetection in embryos injected with the reporter constructs α-tub::GFP or pendrin::GFP, which drive GFP expression in committed MCCs and ionocytes, respectively (Quigley et al., 2011; Stubbs et al., 2006). As shown in Fig. 1B, pSmad1/5/8 immunoreactivity was detected in both MCCs and ionocytes before and after their intercalation into the outer layer. In addition, co-immunostaining for P63 (Tp63 – Xenbase) showed that some pSmad1/5/8-positive inner layer cells were P63 positive (Fig. 1B), revealing that the BMP pathway was active in at least three out of the four currently described cell types born within the inner layer.

In regenerating HAECs, pSMAD1/5 levels increased between the proliferation and polarisation stages, then decreased at the onset of ciliogenesis (Fig. 2A). Although at the polarisation stage the pSMAD1/5 signal was stronger in the apical cell layer of the pluristratified epithelium (Fig. 2B), it increased in the basal layer following treatment with recombinant BMP2 (Fig. 2C,D), showing that basal layer cells were also responsive to the BMP signal.

Thus, BMP pathway activation during the early steps of MCE formation is a conserved feature in our two models. We next addressed the consequences of BMP pathway dysregulation for MCE formation.
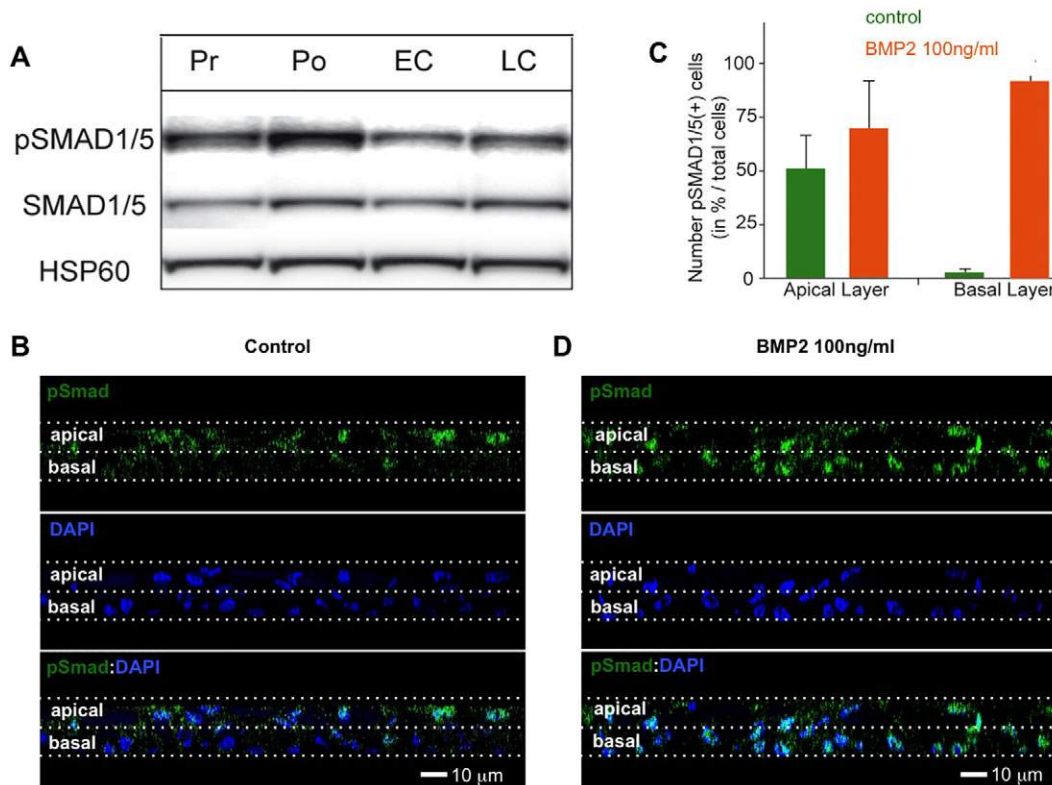
Fig. 2. BMP pathway activity in HAEC cultures. (A) Western blot with an anti-pSMAD1/5 antibody revealed that in HAEC cultures SMAD1/5 phosphorylation increases during the early regeneration stages, then decreases at the onset of ciliogenesis. Pr, proliferation stage (ALI days 0-7); Po, polarising stage (ALI days 7-15); EC, early ciliogenesis (ALI days 15-30); LC, late ciliogenesis (from ALI day 30). HSP60 (HSPD1) was used as a loading control. (B) In HAECs at Po stage, pSMAD1/5 labelling was mostly restricted to apical layer cells. (C,D) The number of pSMAD1/5-positive cells was slightly increased in the apical layer and dramatically increased in the basal layer following a 2 h treatment with BMP2 (100 ng/ml) at Po stage. Data in C are representative of three independent experiments; error bars indicate s.d. (B,D) Orthogonal views (z-slices) of HAECs.

BMP pathway overactivation perturbs the construction of *Xenopus* epidermal and human airway MCE

Injection of stage 9 *Xenopus* embryos with recombinant BMP4 led to increased Smad1/5/8 phosphorylation and nuclear localisation (supplementary material Fig. S1A,B). Scanning electron microscopy (SEM) of the mature epidermis of BMP4-injected embryos revealed a striking decrease in the number of MCCs, ionocytes and SSCs, whereas goblet cells were still apparent (Fig. 3A,A′). *In situ* hybridisation or immunostaining with markers specific for MCCs (α-tubulin and acetylated tubulin; Fig. 3B-C′), ionocytes (*foxi1e* and *v1a*; Fig. 3C-D′) and SSCs (*tph1* and serotonin; Fig. 3E-F′) confirmed the reduction in the numbers of these cell types. Overactivation of the BMP pathway by injection of a constitutively active (CA) form of the BMP receptor Alk3 (Bmpr1a – Xenbase) in ventral ectoderm also led to a decrease in the numbers of MCCs and ionocytes (supplementary material Fig. S2A-C′,D). Surprisingly, a loss of P63 immunoreactivity was observed in BMP-treated embryos (Fig. 3G,G′), suggesting that non-intercalating inner cells were also affected. By contrast, BMP4 treatment did not significantly alter the expression of *otogelin* and *trim29* (Fig. 3H-J′), and rather upregulated *intelectin-1* expression (Fig. 3G,G′), suggesting that goblet cell identity was maintained.

Although the epidermis occasionally appeared thicker in sections of BMP-injected embryos, immunostaining against phospho-histone H3 did not reveal any consistent variation in the number of mitotic nuclei (supplementary material Fig. S2F-H). We next tested whether the observed lack of differentiation of intercalating cells resulted from an earlier defect in specification. For this, we

analysed how BMP treatment affected the expression, prior to intercalation, of *foxj1*, *foxi1e* and *foxa1*, which label committed MCCs, ionocytes and SSCs, respectively. As shown in Fig. 3K-M′, BMP4 injection at stage 9 resulted in a drastic decrease in the early expression levels of these three markers, revealing a defect in the specification of inner intercalating cell types.

In HAECs, chronic treatment with recombinant BMP2 strongly reduced the number of MUC5AC-positive goblet cells, both at polarisation and late ciliogenesis stages (Fig. 4A-B). Likewise, BMP2 treatment suppressed MCCs, as revealed by the absence of acetylated tubulin-positive cells at the late ciliogenesis stage (Fig. 4A-B). Following BMP2 treatment, the cells presented a flattened aspect, reminiscent of the morphology observed in squamous metaplasia, a common alteration of the human upper airway lining (data not shown). Consistent with this interpretation, BMP2-treated HAECs exhibited increased levels of transglutaminase 1 (TGM1) and involucrin (IVL), two markers of squamous metaplasia (Gray et al., 2007; Tanabe et al., 2012) (Fig. 4C).

We conclude that BMP pathway overactivation is incompatible with the construction of a normal MCE in both models. We next addressed the consequences of BMP inhibition in this process.

BMP pathway inhibition perturbs the construction of *Xenopus* epidermal and human airway MCE

Inhibition of the endogenous BMP pathway in the *Xenopus* non-neural ectoderm was achieved by knocking down BMP2, BMP4 and BMP7 with specific morpholino oligonucleotides (BMP MOs), as previously reported (Reversade et al., 2005). In all subsequent
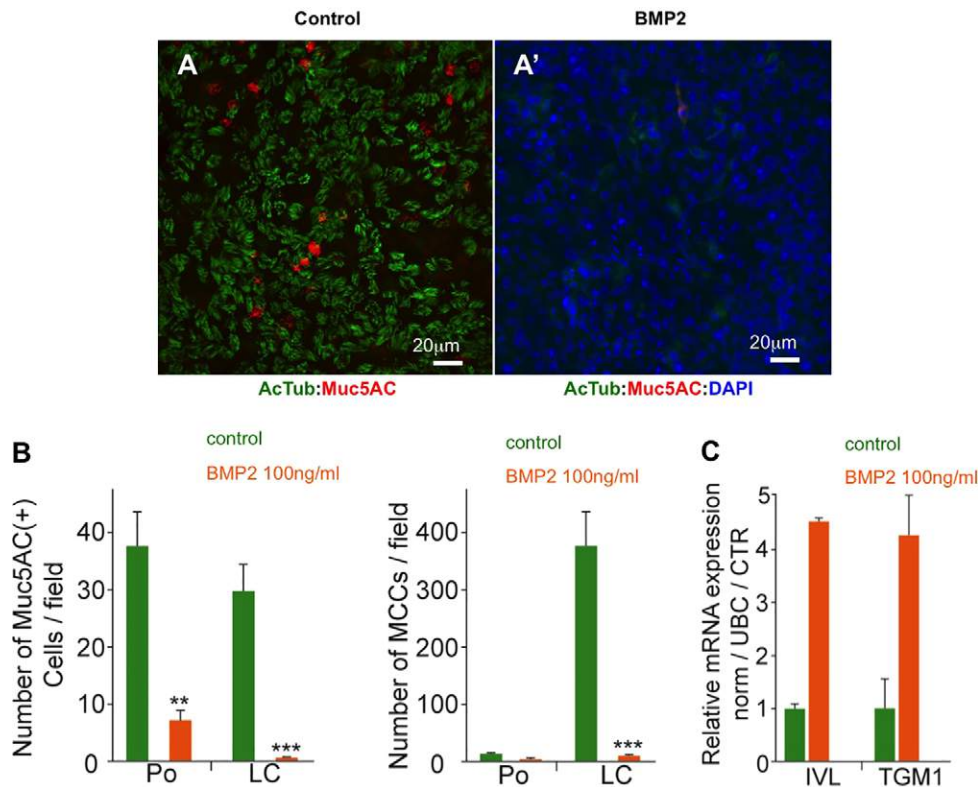
DEVELOPMENT

Fig. 3. BMP pathway overactivation affects cell specification in the developing *Xenopus* epidermis. Stage 9 *Xenopus* embryos were injected in the blastocoel with either BSA (A-M) or 2-7 ng recombinant BMP4 (A′-M′). (A,A′) SEM of the epidermis at stage 37 revealed the severe decrease in the numbers of MCCs (red arrowhead), ionocytes (yellow arrowhead) and SSCs (green arrowhead). (B,B′) At tailbud (stage 30), BMP4-injected embryos showed normal morphology but substantially fewer *α-tubulin*-positive MCCs, as revealed by whole-mount *in situ* hybridisation (WISH). (C,C′) Both the differentiated MCC marker acetylated tubulin (white) and the ionocyte marker *foxi1e* (green) were lost in sectioned tailbud (stage 25) BMP4-injected embryos. (D,D′) WISH revealed that the differentiated ionocyte marker *v1a* was strongly decreased in stage 25 BMP4-injected embryos. (E-F′) The differentiated SSCs markers serotonin (red in E,E′) and *tryptophan hydroxylase-1* (*tph1*, red in F,F′) were lost or strongly decreased in stage 25 BMP4-injected embryos. (G,G′) In sections of stage 25 BMP4-injected embryos, P63 (white), a marker of the non-intercalating inner layer cells, was lost, whereas the goblet cell marker *intelectin-1* (green) was upregulated. *otogelin* (red in H,H′,J,J′) and *trim29* (red in I,I′), two other markers of goblet cells, were unaffected. (K-M′) Stage 14 embryos were analysed by WISH in order to stain MCCs for *foxj1* (K,K′), ionocytes for *foxi1e* (L,L′) and SSCs for *foxa1* (M,M′). (B,B′,D-F′,J-M′) Whole-mount embryos; (C,C′,G-I′) cryosectioned embryos. (B-M′) All markers were revealed by chromogenic or fluorescent *in situ* hybridisation, except for acetylated tubulin, serotonin and P63, which were revealed by immunofluorescence. (C,C′,E-I′) Nuclei were stained with DAPI. (B,B′,D-F′,K-M′) The number of embryos showing the phenotype among the total number of embryos examined is indicated.

experiments, BMP MOs were injected into 8-cell stage animal ventral blastomeres that are fated to become epidermis, together with membrane GFP (mGFP) RNA to visualise and count injected cells. We first verified that BMP MOs suppressed Smad1/5/8 phosphorylation in injected cells (supplementary material Fig. S1C).

BMP MO injection resulted in an increase in the numbers of inner layer cells expressing early markers of MCCs (*foxj1* and *multicilin/MCI*; Fig. 5A-B′) and ionocytes (*foxi1e*; Fig. 5C,C′). A corresponding increase in the number of committed MCCs and ionocytes was visible at tailbud stage (Fig. 5G-I′,P,Q). Injection in the presumptive epidermis of synthetic mRNAs encoding dominant-negative (dn) forms of the BMP receptor Alk3 or the Smad5 transcriptional effector also resulted in an expansion of the MCC and ionocyte populations (supplementary material Fig. S2A″-E). BMP knockdown also caused a significant expansion of SSCs marked early by *foxa1* (Fig. 5D,D′) and in stage 35 tadpoles by *tph1* (Fig. 5R and Fig. 6I-J′).

Unexpectedly, transverse sections through BMP morphant tailbud embryos revealed that *α-tubulin*-positive cells remained trapped between the two layers of the epidermis and failed to produce cilia (Fig. 6A-C′,F-H′,K-M′). The failure of MCCs to intercalate was not simply due to a developmental delay, as most remained trapped below the surface layer in late tadpoles (Fig. 6F-H′,K-M′). MCCs also displayed incomplete intercalation in dnSmad5-injected embryos, although this defect was not as pronounced as in BMP morphants (supplementary material Fig. S1E). An analogous failure to intercalate was observed for ionocytes and SSCs in stage 25 and stage 35 BMP morphants, respectively (Fig. 6D-E′,I-J′).

Finally, BMP MO injection also resulted in lower levels of expression of the goblet cell markers *otogelin* and *trim29* at stage 14 (Fig. 5E-F′), as well as of the 5G7 antigen and *intelectin-1* at stage 25 (Fig. 5J-L′). No statistically significant variation in the number of P63-positive non-intercalating inner cells was observed (Fig. 5S), but these cells displayed lower levels of P63 and *α-dystroglycan* (Fig. 5M-O′).

Fig. 4. BMP pathway overactivation affects the formation of MCCs and mucus-producing cells in HAEC cultures. (A,A′) Chronic treatment of HAEC cultures with 100 ng/ml BMP2 drastically decreased the numbers of both MUC5AC-positive goblet cells and acetylated tubulin-positive MCCs relative to untreated controls. DAPI was added to confirm the presence of cells (A′). (B) Quantification of the experiments illustrated in A,A′ performed in triplicate; data show mean± s.d. from three donors; ***$P<0.001$, **$P<0.01$, Student's t-test. (C) HAECs chronically exposed to 100 ng/ml BMP2 upregulated the squamous metaplasia markers involucrin (IVL) and transglutaminase 1 (TGM1). CTR, control; UBC, ubiquitin C.

In HAECs, BMP inhibition was achieved through chronic treatment with recombinant Noggin protein, a potent secreted BMP antagonist, or with the pharmacological BMP pathway inhibitor dorsomorphin (Yu et al., 2008). We first verified that Noggin could suppress BMP-induced SMAD1/5 phosphorylation and nuclear translocation (supplementary material Fig. S3A,B). Noggin treatment led to a dramatic dose-dependent increase in the number of MCCs (Fig. 7A,B,D-F; supplementary material Fig. S3C). A similar induction was seen upon dorsomorphin treatment (Fig. 7C,F). Fluorescence-activated cell sorting (FACS) confirmed that the number of acetylated tubulin-positive MCCs and MUC5AC-positive goblet cells was increased by ∼4-fold by Noggin (Fig. 7G). The effect of Noggin was strongest when treatment started around the polarisation stage, when BMP pathway activation was maximal (Fig. 2A), and a single 3-day-long pulse of Noggin was sufficient to massively stimulate MCC differentiation (Fig. 7H).

In cystic fibrosis (CF), chronic injuries of the airways lead to epithelium remodelling that is characterised by mucous secretory hyper/metaplasia and a progressive loss of MCCs, dramatically impairing mucociliary clearance and airway defence (Livraghi and Randell, 2007). Thus, we examined whether BMP pathway inhibition by Noggin treatment was also capable of inducing an increase in the number of MCCs in primary cultures derived from CF patients. Fig. 7I-K shows that the effect of Noggin was maintained in CF primary cultures, suggesting that BMP pathway inhibition might stimulate MCC formation and improve mucociliary clearance in chronic airway disease patients.

The BMP and Delta/Notch pathways are linked in the *Xenopus* epidermis

Since the Delta/Notch pathway controls the numbers of MCCs and ionocytes in the *Xenopus* epidermis (Deblandre et al., 1999; Hayes et al., 2007; Quigley et al., 2011; Stubbs et al., 2006), we speculated

that the BMP signal might act through this pathway. Injection of recombinant BMP4 into blastula stage 9 embryos resulted in a strong and persistent upregulation of the Notch ligand *dll1* throughout the ectodermal inner layer (Fig. 8A-D′,H-I″). Conversely, when presumptive epidermal blastomeres were injected with GFP mRNA together with either dnSmad5 mRNA or BMP MOs, a consistent cell-autonomous repression of *dll1* expression was observed compared with embryos injected with GFP mRNA alone (Fig. 8E-G′; data not shown). This was accompanied by an increase in *dll1* expression in some adjacent uninjected cells, most likely owing to reduced activation of the Notch pathway in these cells by the injected cells that contained less Dll1 ligand (Fig. 8E-G′). Strikingly, the ability of exogenous BMP to upregulate *dll1* transcription was temporally limited and coincided with its capacity to suppress MCC, ionocyte and SSC fates. Indeed, as shown in Fig. 8H-J″, blastocoel injection of BMP4 at stage 9 resulted in both *dll1* upregulation at stage 12 and loss of α-tubulin at stage 25, whereas both markers were unaffected when the injection was performed at gastrula stage 11. Interestingly, BMP4 injection at stage 11 did not prevent the normally specified inner cells from reaching the superficial layer (data not shown).

To confirm that the control of *dll1* expression by the BMP pathway was compatible with the observed effect of BMP overexpression on MCCs, ionocytes and SSCs, we examined *dll1* expression relative to early markers of these three cell types. We found that, during gastrulation, *dll1* was first co-expressed with the MCC marker *foxj1*, and soon after with the ionocyte marker *foxi1e* (Fig. 8K-R). This is consistent with the comparable effects produced by Notch pathway activation and repression on the number of both MCCs and ionocytes (Deblandre et al., 1999; Hayes et al., 2007; Quigley et al., 2011; Stubbs et al., 2006). Co-expression of *dll1* and the early SSC marker *foxa1* was also observed at early neurula stage 14 (Fig. 8S-V), consistent with the repression of *foxa1*
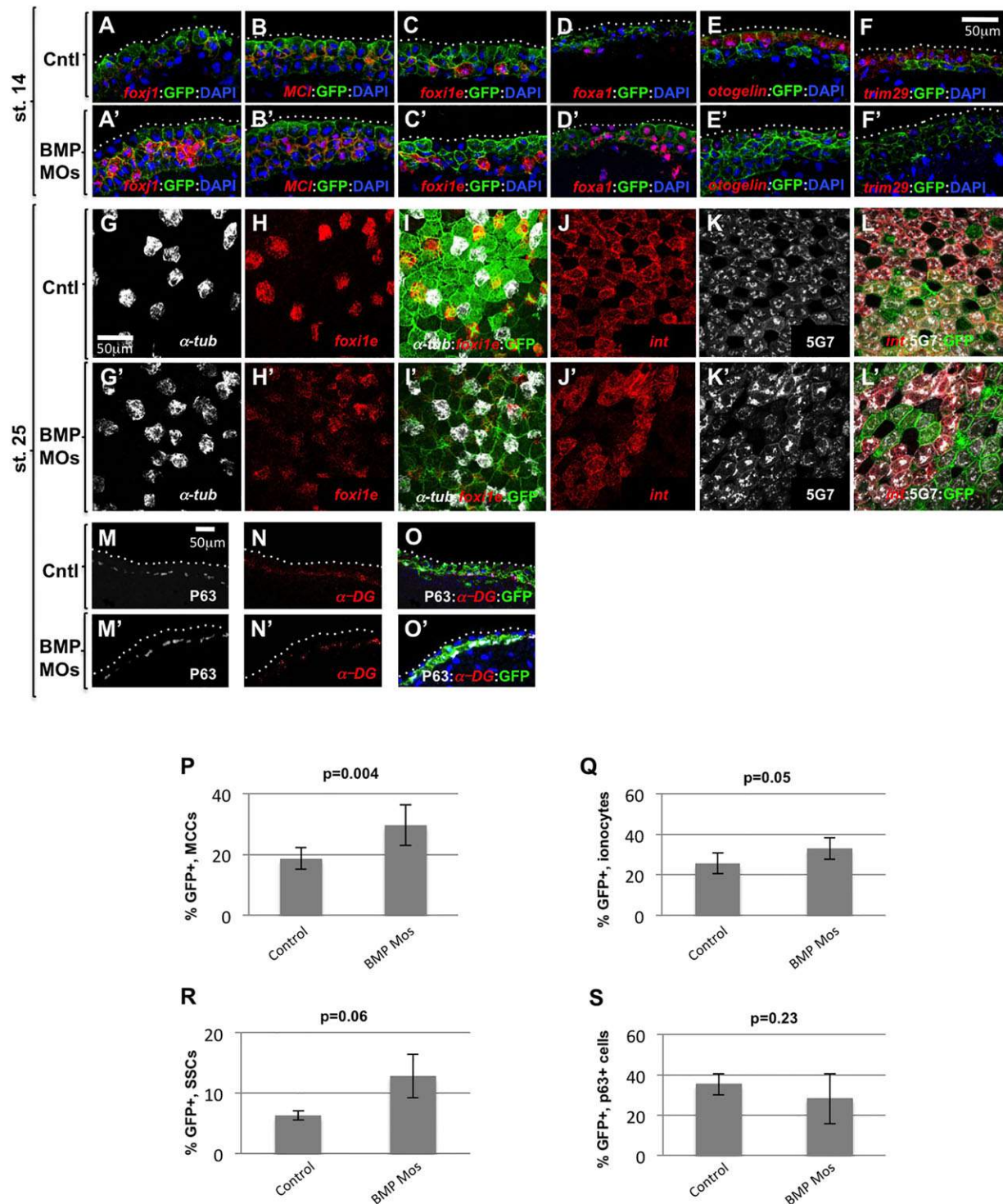
Fig. 5. BMP inhibition promotes MCC, ionocyte and SSC fates in the developing *Xenopus* epidermis. (A-O′) Eight-cell stage *Xenopus* embryos were injected in one animal ventral blastomere (fated to become only epidermis) with either 500 pg GFP mRNA alone (Cntl) or with 500 pg GFP mRNA and BMP2, BMP4 and BMP7 morpholinos (BMP MOs, 10 ng each) and were analysed at stage 14 (A-F′) or 25 (G-O′). GFP immunostaining was used to identify the injected cells. Injection of BMP MOs resulted in an increase in the numbers of stage 14 inner layer cells expressing markers for committed MCCs (*foxj1* and *MCI*, red in A,A′ and B,B′, respectively), for committed ionocytes (*foxi1e*, red in C,C′) and for committed SSCs (*foxa1*, red in D,D′). Conversely, injection of BMP MOs led to a severe decrease in the expression levels of the goblet cell markers *otogelin* and *trim29* (red in E,E′ and F,F′, respectively). When analysed at stage 25, embryos injected with BMP MOs showed an increase in the numbers of both *α-tubulin*-positive MCCs (white in G,G′,I,I′) and *foxi1e*-positive ionocytes (red in H,H′,I,I′), together with a decrease in the expression levels of the outer layer goblet cell markers *intelectin-1* (red in J,J′.L,L′) and 5G7 (white in K-L′) and of the inner layer non-intercalating cell markers P63 (white in M,M′,O,O′) and *α-dystroglycan* (red in N,N′,O,O′). (A-F′,M-O′) Cryosectioned embryos; (G-L′) Whole-mount embryos. (P-S) Quantification of the different inner layer cellular populations in injected epidermal clones at stage 25. Shown are the percentages of MCCs (P), ionocytes (Q), SSCs (R) and P63-positive inner non-intercalating cells (S) among injected, GFP-positive cells. The increase in the number of MCCs, ionocytes and SSCs in BMP morphants was significant (Student's *t*-test). No significant variation was observed for P63-positive cells. Error bars indicate s.d.
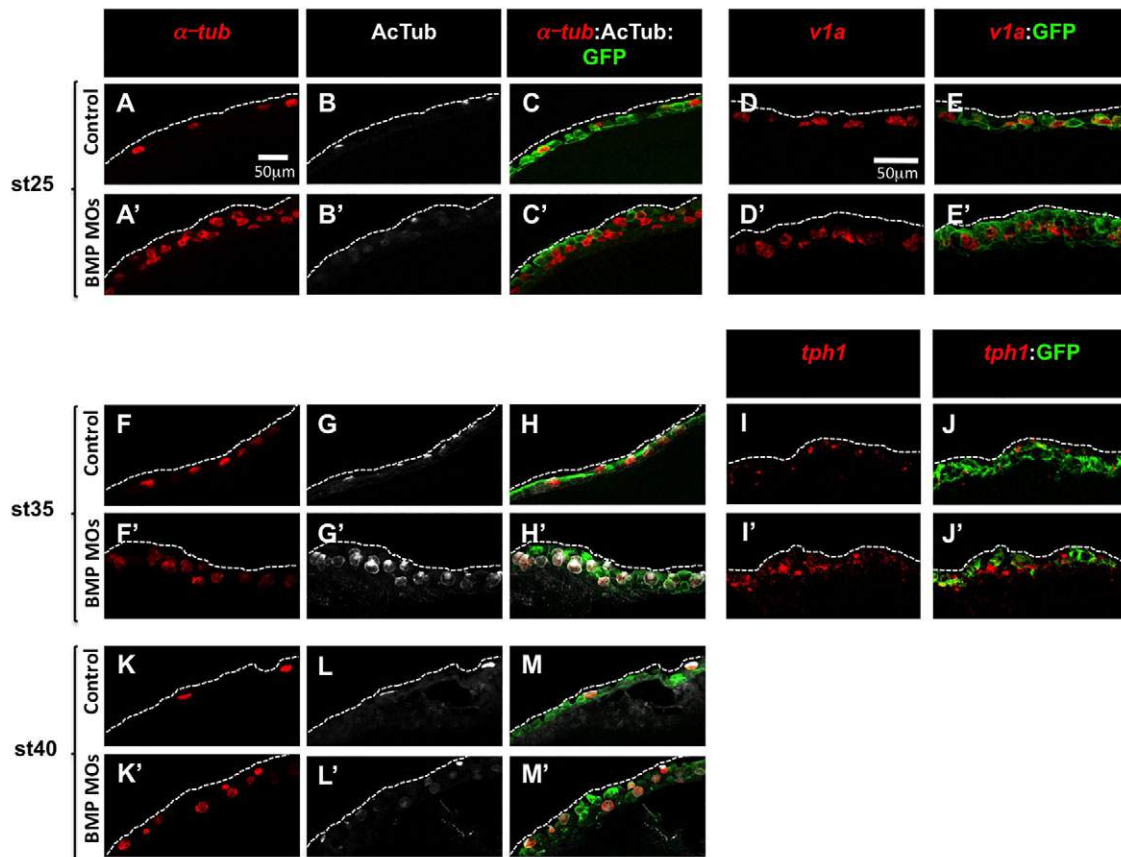
Fig. 6. BMP inhibition prevents the intercalation of MCCs, ionocytes and SSCs in the outer layer of the developing *Xenopus* epidermis. (A-E′) Sectioning through the epidermis at stage 25 revealed that in the BMP MO-injected embryos the supernumerary *α-tubulin*-positive MCCs (red in A-C′) and *v1a*-positive ionocytes (red in D-E′) fail to intercalate into the epidermis outer layer. (I-J′) Likewise, the supernumerary *tph1*-positive SSCs failed to intercalate in stage 35 BMP morphants (red in I-J′). (F-H′,K-M′) Even at later developmental stages, most of the supernumerary MCCs, which expressed the differentiation marker acetylated tubulin (white), were unable to intercalate properly into the outer layer.

expression in Notch intracellular domain (NICD)-injected embryos (Hayes et al., 2007).

In summary, tightly regulated BMP activity appears to be required for *dll1* expression and the specification of MCCs, ionocytes, SSCs and non-intercalating inner cells, presumably through the Notch pathway. Consistent with this view, injection of a dominant-negative form of the Notch effector Su(H) was able to limit the decrease in MCC specification caused by a constitutively active form of the BMP receptor, while a constitutively active form of Su(H) was able to counteract the increase in MCC specification produced by a dominant-negative form of the BMP receptor (supplementary material Fig. S4).

DISCUSSION

Our study reveals that the construction of MCE in two distant vertebrate models commonly involves the BMP signalling pathway. Below, we highlight similarities and differences between the responses to BMP modulation in our two models.

In *Xenopus* epidermis, we found that exogenous BMP4 prevents the specification of MCCs, ionocytes, SSCs and P63-positive non-intercalating inner cells. In other words, all inner cell fates are suppressed when BMP is over-active. By contrast, outer layer goblet cells are specified normally. Conversely, BMP pathway inhibition leads to an increase in the numbers of MCCs, ionocytes and SSCs, but not P63-positive cells, and antagonises goblet cell differentiation. In HAECs, both goblet and MCC fates are suppressed by exposure to

exogenous BMP2 protein, and both fates are induced by BMP inhibition. Thus, goblet cells exhibit opposite responses to BMP in our two systems. This is likely to reflect the difference in the goblet cell lineage in the two models. In HAECs, goblet cells and MCCs are likely to derive from common P63-positive progenitors (Hogan et al., 2014), and it seems logical that they exhibit similar responses to BMP modulation. In the *Xenopus* epidermis, goblet cells are born in the outer layer whereas MCCs are born in the inner layer. The two layers of the epidermis are produced through oriented cell divisions during cleavage stages and inherit different maternal determinants that control inner and outer cell fates (Chalmers et al., 2003; Ossipova et al., 2007). Thus, goblet cells and MCCs are born from lineages that have been separated before the activation of the zygotic genome, which might explain why they respond in an opposite manner to the zygotic inducer BMP. The *Xenopus* embryonic epidermis also contains ionocytes, which are involved in osmoregulation (Dubaissi and Papalopulu, 2011; Quigley et al., 2011), and SSCs, which control the ciliary beating frequency of MCCs and secrete anti-infective substances that protect the embryo (Dubaissi et al., 2014; Walentek et al., 2014). Ionocytes and SSCs have no clear counterparts in human airways, so no pertinent comparison can be made.

The most striking parallel between our two models is the identical response of MCCs to BMP pathway modulation. This observation is consistent with multiple reports of common molecular mechanisms at the basis of MCC differentiation in vertebrates (Boon et al., 2014; Marcet et al., 2011; Song et al., 2014; Stubbs et al., 2012; Tan et al.,
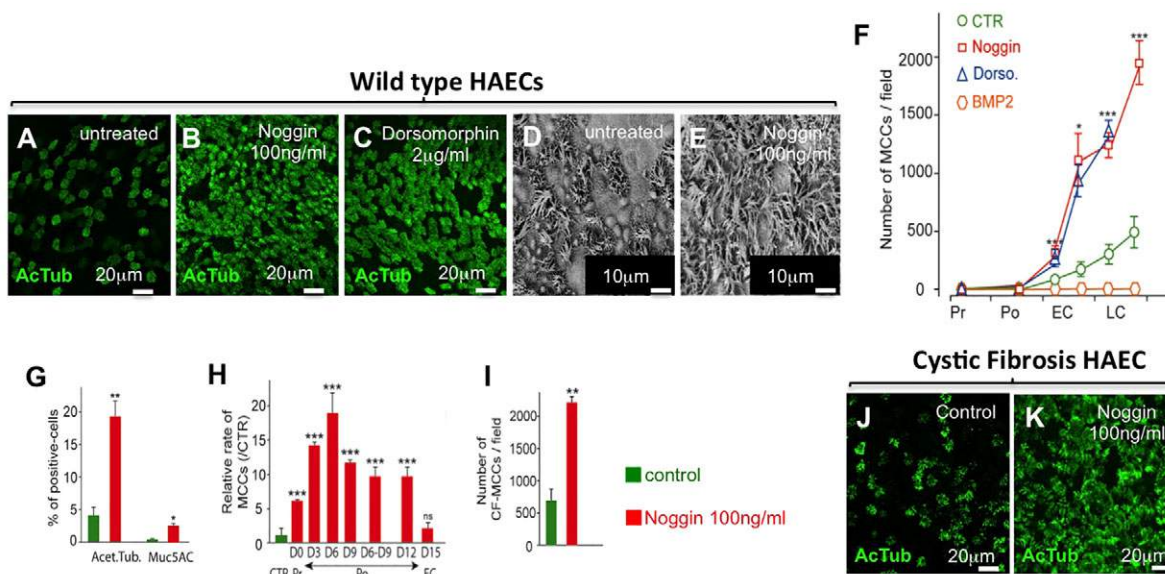
Fig. 7. BMP inhibition promotes the MCC fate in regenerating HAECs. (A-C,J,K) Acetylated tubulin-positive, morphologically normal MCCs increased following BMP pathway inhibition by treatment with Noggin (100 ng/ml) in HAEC cultures from healthy donors (A-C) or cystic fibrosis patients (J,K). (D,E) SEM images of control or Noggin-treated HAEC cultures at stage LC. (F) The number of MCCs per field of observation in HAEC cultures from three donors at various time points of culture. Noggin and dorsomorphin (Dorso.) induced precocious and increased rates of ciliogenesis. CTR, control (G) FACS confirmed the increase in MCCs and goblet cells in Noggin-treated normal HAEC cultures. (H) The maximal increase in the number of MCCs relative to untreated cultures was observed when Noggin treatment of HAECs started at Po stage (ALI days 6-9). (I) Noggin treatment increases the number of MCCs in HAEC cultures from cystic fibrosis (CF) donors. (G-I) Data are mean±s.d. from three independent experiments; *P<0.05; **P<0.01; ***P<0.001; ns, not significant; Student's t-test.

2013; Wallmeier et al., 2014). We conclude that, at the present time, the comparison between HAEC cultures and the developing *Xenopus* embryonic epidermis is mostly relevant to an understanding of MCC biology.

Recent studies have developed protocols to generate *in vitro* airway epithelial cells from human pluripotent stem cells that include an early inhibition of the BMP pathway followed by its activation in order to push the definitive endoderm to differentiate into ventral anterior foregut, before the induction of lung progenitor specification (Firth et al., 2014; Huang et al., 2015, 2014). However, these reports did not explore the role of BMP signalling at later steps, when airway progenitors give rise to fully differentiated airway MCE. Our work reveals that BMP inhibition may facilitate the commitment of multipotent airway progenitors towards MCC and goblet cell fates, making it an important signalling pathway to be considered for human airway regeneration in physiological as well as pathological situations.

The activity of the BMP pathway, which is initially required for the partitioning of the non-neural ectoderm in *Xenopus* (De Robertis, 2006) and for lung morphogenesis in mammals (Huang et al., 2014; Mou et al., 2012; Sountoulidis et al., 2012), has subsequently to be tightly controlled to ensure MCE formation. In the developing epidermis, all cell types appear to experience BMP pathway activity, although cell type-specific differences in the timing or strength of the signal cannot be ruled out. The temporal window of susceptibility of the developing *Xenopus* ectoderm to exogenous BMP4 ends by mid-gastrula stage 11. Interestingly, this stage is known to mark the end of the temporal window of competence of embryonic cells to respond to exogenous inducers (Snape et al., 1987; Wylie et al., 1987). This observation indicates that the BMP signal exerts its action on an early pool of multipotent inner layer cells, which will give rise to MCCs, ionocytes, SSCs and P63-positive cells. Thus, the BMP signal might not instruct cell fates, but rather promotes in the non-neural ectoderm a permissive state compatible with fate choices by downstream regulators. In HAEC cultures, the BMP treatment almost completely obliterates the formation of both MCCs and goblet cells and results in the expression of markers of squamous epithelia. This is reminiscent of the squamous metaplasia that occurs when the airway epithelium is submitted to chronic damage or irritation and might reflect the excessively prolonged maintenance of the cells in an uncommitted state (Hogan et al., 2014). Altogether, our data suggest that, in developing or regenerating vertebrate MCE, fate commitment cannot be initiated when BMP activity is too high. We propose that attenuation of BMP activity, by as yet unknown mechanisms, is required for cells to engage in fate choices.

We found that BMP signalling is required to activate *dll1* expression in the *Xenopus* developing epidermis, although the absence of clear Smad consensus binding sites upstream of the *dll1* open reading frame (data not shown) suggests an indirect mode of control. The decreased *dll1* expression in the absence of BMP is expected to reduce Notch activation and allow a greater number of cells to engage in intercalating cell fate choices. In agreement with this interpretation, Dll1 knockdown induces supernumerary MCCs (Marcet et al., 2011). By contrast, the strong and persistent induction of *dll1* expression in BMP4-injected embryos was correlated with the lack of specification of all inner cell types. This finding is at odds with the published observation that injection of a synthetic *dll1* mRNA leads to an increase in the number of MCCs, presumably through cis-inhibition of Notch (Deblandre et al., 1999). Thus, Notch cis-inhibition by increased levels of *dll1* transcripts might not occur in the presence of excess BMP activity. Conversely, increased *dll1* expression in BMP4-injected embryos might not translate into Notch activation either, as it should otherwise induce P63 expression (Sirour et al., 2011). We conclude that BMP overactivation produces inhibitory effects that make it impossible for inner layer cells to initiate their specification programme. Such inhibitory effects might include the artificial
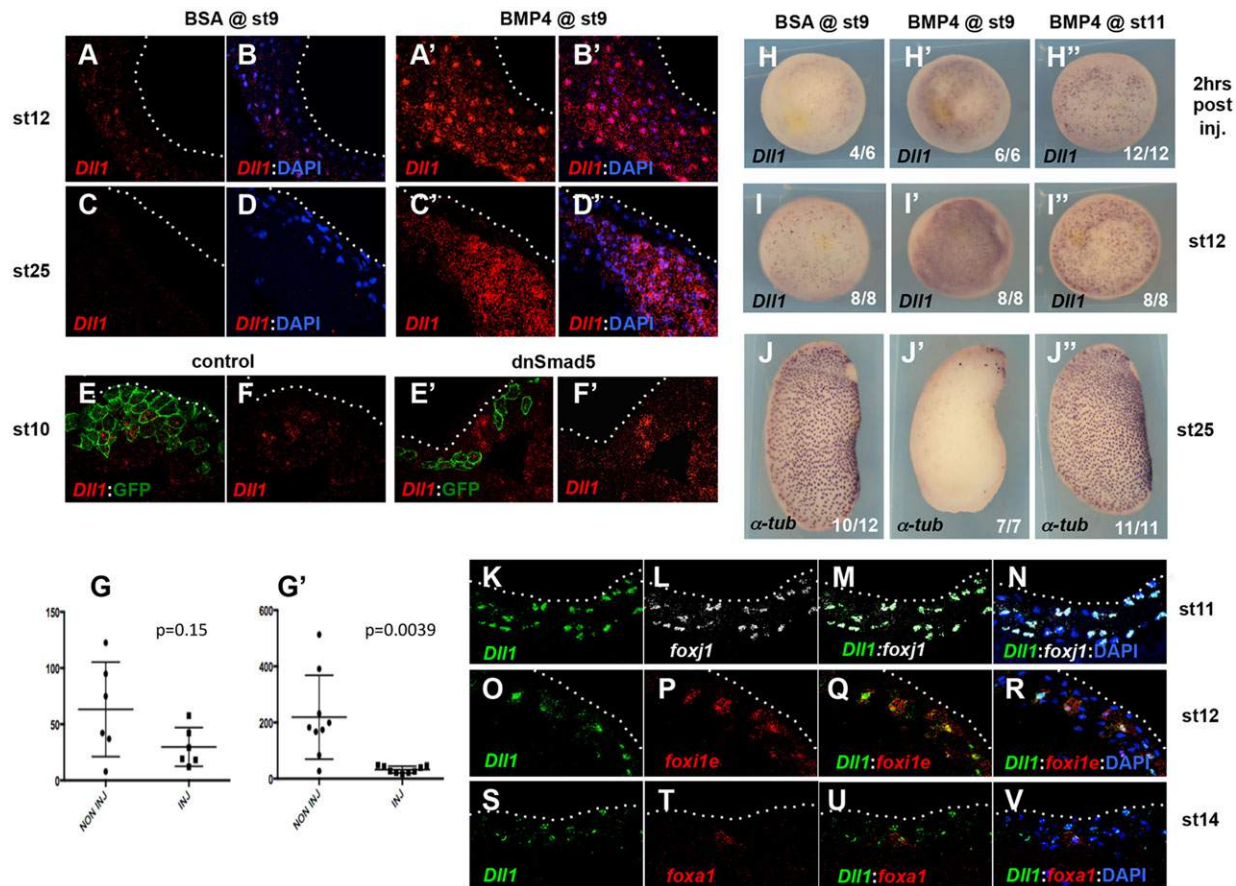
Fig. 8. The BMP pathway controls *dll1* expression in the developing *Xenopus* epidermis. (A-D′) Embryos injected in the blastocoel at stage 9 with either BSA or BMP4 were probed for *dll1* expression at stage 12 or 25. BMP4-injected embryos showed a strong and persistent upregulation of *dll1* within the epidermal inner layer. (E-F′) Eight-cell stage embryos were injected in a ventral ectoderm precursor blastomere with GFP mRNA alone (control) or with GFP mRNA and an mRNA encoding dominant-negative Smad5 (dnSmad5). Stage 10 embryos were sectioned and hybridised with a probe against *dll1* and an antibody against GFP. The amount of *dll1* signal (red) that colocalised with GFP fluorescence (green) was lower when GFP was co-injected with dnSmad5, indicating that dnSmad5 cell-autonomously decreases *dll1* expression. (G,G′) The *dll1* signal (red channel fluorescence) was measured in areas of equal size within (inj) or outside (non inj) of the injected clones in control (G) and dnSmad5-injected (G′) embryos. Signals were compared pairwise within each section, confirming the significant decrease in *dll1* signal in dnSmad5-injected cells (Wilcoxon test). The middle bar indicates the median, and the outlier bars delimit the lower and upper quartiles. (H-J″) Embryos were injected at stage 9 with BSA (H,I,J), or with BMP4 at stage 9 (H′,I′,J′) or 11 (H″,I″,J″), then probed for *dll1* 2 h after injection (H-H″) or at stage 12 (I-I″) and for α-tubulin at stage 25 (J-J″). BMP4 caused ectopic *dll1* activation and the loss of MCCs when injected at stage 9 but not at stage 11. (K-V) Cryosectioned embryos were hybridised with probes against *dll1* and the MCC early marker *foxj1* (K-N), the ionocyte early marker *foxi1e* (O-R) or the SSC early marker *foxa1* (S-V) at stages 11, 12 and 14, respectively. *dll1* colocalised with *foxj1* at stage 11, with *foxi1e* at stage 12 and with *foxa1* at stage 14.

maintenance of pluripotency regulators by excess BMP activity (Morrison and Brickman, 2006; Scerbo et al., 2012; Ying et al., 2003). However, the inhibition caused by BMP may be overcome, to a certain extent, by the Notch pathway, as suggested by the antagonism observed when the BMP and Notch pathways were concomitantly manipulated in opposite ways (supplementary material Fig. S4).

Following their specification in the inner epidermal layer, the MCCs, ionocytes and SSCs migrate to the outer layer, where they intercalate among goblet cells, a morphogenetic step crucial for the development of the functional *Xenopus* epidermis, but which has no clear counterpart in the regenerating HAEC cultures. Our data show that blocking the BMP signal by injection of BMP MOs completely and durably prevents intercalation of MCCs, ionocytes and SSCs. The failure in intercalation might depend non-exclusively on a cell-autonomous disruption of cytoskeleton dynamics in intercalating cells, or on defects in the differentiation of the inner and/or outer layer cells that render the epidermal environment non-permissive for intercalation. Although this

issue deserves further investigation, it is remarkable that the transmembrane protein α-Dystroglycan, which is expressed by inner non-intercalating cells and is downregulated following BMP knockdown, has been shown to be required for MCC intercalation (Sirour et al., 2011).

Thus, in the *Xenopus* epidermal MCE, BMP activity coordinates cell fate specification with cell movement. It is important to stress that this dual role was not reported for the Notch pathway, as supernumerary MCCs induced by Notch inhibition in the epidermis do manage to intercalate (Deblandre et al., 1999; Stubbs et al., 2006).

In conclusion, our study reveals that vertebrate MCE construction involves the BMP pathway at multiple steps of the organogenetic process. Beyond the global overview provided by this study, more focused analyses will be required to understand how BMP activity is spatially and temporally controlled, to identify at the molecular level the responses induced by BMP modulation, and to decipher the complex interplay with other signalling pathways.

MATERIALS AND METHODS

Human tissue samples

Inferior turbinates or nasal polyps were from patients who underwent surgical intervention for nasal obstruction or septoplasty (kindly provided by Prof. Castillo, Pasteur Hospital, Nice, France). Samples from CF patients were purchased from Epithelix Sarl (Geneva, Switzerland). The use of human tissues was authorised by bioethics law 94-654 of the French Public Health Code after written consent from the patients.

Ethics statement

Isolation and culture of human airway epithelial cells

Primary HAEC cultures were performed according to Marcet et al. (2011). HAEC differentiation was analysed at four time points following exposure of HAECs at an air-liquid interface (ALI). Pr, Po, EC and LC represent the proliferating step at ALI day 0, the polarisation step at ALI day 7, the early multiciliogenesis step at ALI day 14 and the late multiciliogenesis step at ALI day 21, respectively.

General *Xenopus* procedures

Eggs obtained from NASCO females were fertilised *in vitro*, dejellied, cultured and injected as described previously (Marchal et al., 2009). Synthetic capped mRNAs were produced with the Ambion mMESSAGE mMACHINE Kit. BMP2, BMP4 and BMP7 morpholinos were described by Reversade et al. (2005). Recombinant zebrafish Bmp4 protein was resuspended as recommended by the manufacturer (R&D Systems, catalogue number 1128-BM), and injected through the animal pole into the blastocoelic cavity of embryos at blastula or at gastrula stages. Plasmids for the MCC α-tub::GFP and ionocyte pendrin::GFP reporter constructs were linearised by *Sal*I and injected into one animal cell at the 8-cell stage.

Stainings

Xenopus

Whole-mount chromogenic *in situ* hybridisation was performed as described previously (Marchal et al., 2009). Whole-mount fluorescent *in situ* hybridisation (FISH) was performed as described previously (Castillo-Briceno and Kodjabachian, 2014). For single staining, all RNA probes were labelled with digoxigenin. For double staining, *dll1* was labelled with fluorescein, *foxa1* and *foxi1e* with digoxigenin, and *foxj1* with DNP. Sections for FISH or immunohistochemistry (IHC) were prepared as follows. Embryos were fixed in either 4% formaldehyde or paraformaldehyde (PFA), stored in methanol for at least 4 h at −20°C, then rehydrated in PBT (PBS+Tween 0.1% v/v), treated with triethanolamine and acetic anhydride, incubated in increasing sucrose concentrations and finally embedded with OCT (VWR Chemicals). 12-μm-thick cryosections were created. FISH on sections was an adaptation of the whole-mount FISH method. Immunohistochemical staining was performed on whole embryos as described previously (Castillo-Briceno and Kodjabachian, 2014) and adapted for sections.

Human

Fresh cultures of ALI-D28 (LC) HAECs were used for immunodetection as previously described (Marcet et al., 2011). Cells were fixed (4% PFA, 15 min, 4°C), rinsed (0.1 M glycine in PBS, 10 min) and permeabilised (0.1% Triton X-100, 5 min). Fixed cells were blocked for 1 h in 3% BSA, and incubated for 1 h at room temperature or overnight at 4°C with the appropriate primary antibodies (supplementary material Table S1). Then, cells were incubated for 1 h with the appropriate secondary antibodies (supplementary material Table S1). Stained cells were mounted with ProLong Gold antifade reagent (Invitrogen, Life Technologies). After FISH and IHC, and just before mounting, samples were placed in DAPI (1 μg/ml in PBS) for 3 min for whole *Xenopus* embryos and HAECs and 2 min for sections.

Imaging

Images of HAEC cultures were acquired using an Olympus Fv10i or Leica SP5 confocal imaging system with 60× oil-immersion objective. Epidermal tissue from *Xenopus* embryos was explanted and mounted with Fluoromount G (Fluoprobes) and allowed to dry before imaging on a Zeiss LSM780 confocal microscope. Images were acquired as 8 bit/channel and with 1024×1024 pixel resolution, and processed in ImageJ for maximum intensity z-projection and/or merge of channels. Expression levels on FISH were analysed using ImageJ. For *Xenopus*, stacks of confocal images from four to five explants per experiment and per condition were made. Z-projection of the green channel images was used to count GFP-positive injected cells. MCCs, ionocytes and SSCs were counted using a merge of their corresponding channels with the green channel on order to consider only injected cells. Statistical analysis was made using GraphPad Prism 6.

SEM processing and imaging

Xenopus

Samples were prepared and imaged as previously described (Castillo-Briceno and Kodjabachian, 2014).

Human

SEM was performed at the CCMA EM Core Facility of the University of Nice Sophia-Antipolis. Briefly, cells were fixed in 1.6% glutaraldehyde in 0.1 M phosphate buffer, rinsed and post-fixed 30 min in osmium tetroxide (1% in 0.1 M phosphate buffer). After rinsing, cells were dehydrated in a graded ethanol series and dried using hexamethyldisilazane (HMDS). Cells were mounted on aluminium stubs with adhesive tabs, sputter-coated with Pt (Cressington, 308R) and examined on a 6700F field emission scanning electron microscope (JEOL).

Western blot

Primary HAECs were harvested by scraping in RIPA lysis buffer (Thermo Scientific Pierce) and cleared by centrifugation. Protein concentration was determined using the BCA assay (Thermo Fisher Scientific) and equivalent amounts of protein were resolved by electrophoresis using the Novex NuPAGE SDS-PAGE Gel System following the manufacturer's instructions. Proteins were transferred to PVDF membranes (Bio-Rad) and analysed by immunoblotting with appropriate primary antibodies (supplementary material Table S1) and HRP-conjugated secondary antibodies (1/5000, Dako). Immunoreactive bands were detected using the Immobilon ECL Kit (Merck Millipore) on an LAS-3000 imager (Fujifilm).

Supplementary material

Supplementary material available online at
http://dev.biologists.org/lookup/suppl/doi:10.1242/dev.118679/-/DC1

References

Boon, M., Wallmeier, J., Ma, L., Loges, N. T., Jaspers, M., Olbrich, H., Dougherty, G. W., Raidt, J., Werner, C., Amirav, I. et al. (2014). MCIDAS mutations result in a mucociliary clearance disorder with reduced generation of multiple motile cilia. *Nat. Commun.* **5**, 4418.

Castillo-Briceno, P. and Kodjabachian, L. (2014). Xenopus embryonic epidermis as a mucociliary cellular ecosystem to assess the effect of sex hormones in a non-reproductive context. *Front. Zool.* **11**, 9.

Chalmers, A. D., Strauss, B. and Papalopulu, N. (2003). Oriented cell divisions asymmetrically segregate aPKC and generate cell fate diversity in the early Xenopus embryo. *Development* **130**, 2657-2668.

Chung, M.-I., Kwon, T., Tu, F., Brooks, E. R., Gupta, R., Meyer, M., Baker, J. C., Marcotte, E. M. and Wallingford, J. B. (2014). Coordinated genomic control of ciliogenesis and cell movement by RFX2. *Elife* **3**, e01439.

Cibois, M., Scerbo, P., Thome, V., Pasini, A. and Kodjabachian, L. (2014). Induction and differentiation of the Xenopus ciliated embryonic epidermis. In *Xenopus Development* (ed. M. Kloc and J. Z. Kubiak), pp. 112-129. Oxford: John Wiley & Sons.

De Robertis, E. M. (2006). Spemann's organizer and self-regulation in amphibian embryos. *Nat. Rev. Mol. Cell Biol.* **7**, 296-302.

De Robertis, E. M. and Kuroda, H. (2004). Dorsal-ventral patterning and neural induction in Xenopus embryos. *Annu. Rev. Cell Dev. Biol.* **20**, 285-308.

Deblandre, G. A., Wettstein, D. A., Koyano-Nakagawa, N. and Kintner, C. (1999). A two-step mechanism generates the spacing pattern of the ciliated cells in the skin of Xenopus embryos. *Development* **126**, 4715-4728.

Dubaissi, E. and Papalopulu, N. (2011). Embryonic frog epidermis: a model for the study of cell-cell interactions in the development of mucociliary disease. *Dis. Model. Mech.* **4**, 179-192.

Dubaissi, E., Rousseau, K., Lea, R., Soto, X., Nardeosingh, S., Schweickert, A., Amaya, E., Thornton, D. J. and Papalopulu, N. (2014). A secretory cell type develops alongside multiciliated cells, ionocytes and goblet cells, and provides a protective, anti-infective function in the frog embryonic mucociliary epidermis. *Development* **141**, 1514-1525.

Fahy, J. V. and Dickey, B. F. (2010). Airway mucus function and dysfunction. *N. Engl. J. Med.* **363**, 2233-2247.

Firth, A. L., Dargitz, C. T., Qualls, S. J., Menon, T., Wright, R., Singer, O., Gage, F. H., Khanna, A. and Verma, I. M. (2014). Generation of multiciliated cells in functional airway epithelia from human induced pluripotent stem cells. *Proc. Natl. Acad. Sci. USA* **111**, E1723-E1730.

Gray, A. C., McLeod, J. D. and Clothier, R. H. (2007). A review of in vitro modelling approaches to the identification and modulation of squamous metaplasia in the human tracheobronchial epithelium. *Altern. Lab. Anim.* **35**, 493-504.

Guruharsha, K. G., Kankel, M. W. and Artavanis-Tsakonas, S. (2012). The Notch signalling system: recent insights into the complexity of a conserved pathway. *Nat. Rev. Genet.* **13**, 654-666.

Hajj, R., Baranek, T., Le Naour, R., Lesimple, P., Puchelle, E. and Coraux, C. (2007). Basal cells of the human adult airway surface epithelium retain transit-amplifying cell properties. *Stem Cells* **25**, 139-148.

Hayes, J. M., Kim, S. K., Abitua, P. B., Park, T. J., Herrington, E. R., Kitayama, A., Grow, M. W., Ueno, N. and Wallingford, J. B. (2007). Identification of novel ciliogenesis factors using a new in vivo model for mucociliary epithelial development. *Dev. Biol.* **312**, 115-130.

Hogan, B. L. M., Barkauskas, C. E., Chapman, H. A., Epstein, J. A., Jain, R., Hsia, C. C. W., Niklason, L., Calle, E., Le, A., Randell, S. H. et al. (2014). Repair and regeneration of the respiratory system: complexity, plasticity, and mechanisms of lung stem cell function. *Cell Stem Cell* **15**, 123-138.

Huang, S. X. L., Islam, M. N., O'Neill, J., Hu, Z., Yang, Y.-G., Chen, Y.-W., Mumau, M., Green, M. D., Vunjak-Novakovic, G., Bhattacharya, J. et al. (2014). Efficient generation of lung and airway epithelial cells from human pluripotent stem cells. *Nat. Biotechnol.* **32**, 84-91.

Huang, S. X. L., Green, M. D., de Carvalho, A. T., Mumau, M., Chen, Y.-W., D'Souza, S. L. and Snoeck, H.-W. (2015). The in vitro generation of lung and airway progenitor cells from human pluripotent stem cells. *Nat. Protoc.* **10**, 413-425.

Karp, P. H., Moninger, T. O., Weber, S. P., Nesselhauf, T. S., Launspach, J. L., Zabner, J. and Welsh, M. J. (2002). An in vitro model of differentiated human airway epithelia. Methods for establishing primary cultures. *Methods Mol. Biol.* **188**, 115-137.

Livraghi, A. and Randell, S. H. (2007). Cystic fibrosis and other respiratory diseases of impaired mucus clearance. *Toxicol. Pathol.* **35**, 116-129.

Lu, P., Barad, M. and Vize, P. D. (2001). Xenopus p63 expression in early ectoderm and neurectoderm. *Mech. Dev.* **102**, 275-278.

Lyons, R. A., Saridogan, E. and Djahanbakhch, O. (2006). The reproductive significance of human Fallopian tube cilia. *Hum. Reprod. Update* **12**, 363-372.

Marcet, B., Chevalier, B., Luxardi, G., Coraux, C., Zaragosi, L.-E., Cibois, M., Robbe-Sermesant, K., Jolly, T., Cardinaud, B., Moreilhon, C. et al. (2011).

Control of vertebrate multiciliogenesis by miR-449 through direct repression of the Delta/Notch pathway. *Nat. Cell Biol.* **13**, 1280.

Marchal, L., Luxardi, G., Thome, V. and Kodjabachian, L. (2009). BMP inhibition initiates neural induction via FGF signaling and Zic genes. *Proc. Natl. Acad. Sci. USA* **106**, 17437-17442.

Masterson, J. C., Molloy, E. L., Gilbert, J. L., McCormack, N., Adams, A. and O'Dea, S. (2011). Bone morphogenetic protein signalling in airway epithelial cells during regeneration. *Cell. Signal.* **23**, 398-406.

McCormack, N., Molloy, E. L. and O'Dea, S. (2013). Bone morphogenetic proteins enhance an epithelial-mesenchymal transition in normal airway epithelial cells during restitution of a disrupted epithelium. *Respir. Res.* **14**, 36.

Morrison, G. M. and Brickman, J. M. (2006). Conserved roles for Oct4 homologues in maintaining multipotency during early vertebrate development. *Development* **133**, 2011-2022.

Mou, H., Zhao, R., Sherwood, R., Ahfeldt, T., Lapey, A., Wain, J., Sicilian, L., Izvolsky, K., Lau, F. H., Musunuru, K. et al. (2012). Generation of multipotent lung and airway progenitors from mouse ESCs and patient-specific cystic fibrosis iPSCs. *Cell Stem Cell* **10**, 385-397.

Ossipova, O., Tabler, J., Green, J. B. A. and Sokol, S. Y. (2007). PAR1 specifies ciliated cells in vertebrate ectoderm downstream of aPKC. *Development* **134**, 4297-4306.

Quigley, I. K., Stubbs, J. L. and Kintner, C. (2011). Specification of ion transport cells in the Xenopus larval skin. *Development* **138**, 705-714.

Reversade, B., Kuroda, H., Lee, H., Mays, A. and De Robertis, E. M. (2005). Depletion of Bmp2, Bmp4, Bmp7 and Spemann organizer signals induces massive brain formation in Xenopus embryos. *Development* **132**, 3381-3392.

Rock, J. R., Onaitis, M. W., Rawlins, E. L., Lu, Y., Clark, C. P., Xue, Y., Randell, S. H. and Hogan, B. L. M. (2009). Basal cells as stem cells of the mouse trachea and human airway epithelium. *Proc. Natl. Acad. Sci. USA* **106**, 12771-12775.

Rompolas, P., Azimzadeh, J., Marshall, W. F. and King, S. M. (2013). Analysis of ciliary assembly and function in planaria. *Methods Enzymol.* **525**, 245-264.

Scerbo, P., Girardot, F., Vivien, C., Markov, G. V., Luxardi, G., Demeneix, B., Kodjabachian, L. and Coen, L. (2012). Ventx factors function as Nanog-like guardians of developmental potential in Xenopus. *PLoS ONE* **7**, e36855.

Schohl, A. and Fagotto, F. (2002). Beta-catenin, MAPK and Smad signaling during early Xenopus development. *Development* **129**, 37-52.

Silverman, H., Lynn, J. W., Beninger, P. G. and Dietz, T. H. (1999). The role of latero-frontal cirri in particle capture by the gills of Mytilus edulis. *Biol. Bull.* **197**, 368-376.

Sirour, C., Hidalgo, M., Bello, V., Buisson, N., Darribere, T. and Moreau, N. (2011). Dystroglycan is involved in skin morphogenesis downstream of the Notch signaling pathway. *Mol. Biol. Cell* **22**, 2957-2969.

Snape, A., Wylie, C. C., Smith, J. C. and Heasman, J. (1987). Changes in states of commitment of single animal pole blastomeres of Xenopus laevis. *Dev. Biol.* **119**, 503-510.

Song, R., Walentek, P., Sponer, N., Klimke, A., Lee, J. S., Dixon, G., Harland, R., Wan, Y., Lishko, P., Lize, M. et al. (2014). miR-34/449 miRNAs are required for motile ciliogenesis by repressing cp110. *Nature* **510**, 115-120.

Sountoulidis, A., Stavropoulos, A., Giaglis, S., Apostolou, E., Monteiro, R., Chuva de Sousa Lopes, S. M., Chen, H., Stripp, B. R., Mummery, C., Andreakos, E. et al. (2012). Activation of the canonical bone morphogenetic protein (BMP) pathway during lung morphogenesis and adult lung tissue repair. *PLoS ONE* **7**, e41460.

Stubbs, J. L., Davidson, L., Keller, R. and Kintner, C. (2006). Radial intercalation of ciliated cells during Xenopus skin development. *Development* **133**, 2507-2515.

Stubbs, J. L., Vladar, E. K., Axelrod, J. D. and Kintner, C. (2012). Multicilin promotes centriole assembly and ciliogenesis during multiciliate cell differentiation. *Nat. Cell Biol.* **14**, 140-147.

Tan, F. E., Vladar, E. K., Ma, L., Fuentealba, L. C., Hoh, R., Espinoza, F. H., Axelrod, J. D., Alvarez-Buylla, A., Stearns, T., Kintner, C. et al. (2013). Myb promotes centriole amplification and later steps of the multiciliogenesis program. *Development* **140**, 4277-4286.

Tanabe, T., Kanoh, S., Moskowitz, W. B. and Rubin, B. K. (2012). Cardiac asthma: transforming growth factor-beta from the failing heart leads to squamous metaplasia in human airway cells and in the murine lung. *Chest* **142**, 1274-1283.

Walentek, P., Bogusch, S., Thumberger, T., Vick, P., Dubaissi, E., Beyer, T., Blum, M. and Schweickert, A. (2014). A novel serotonin-secreting cell type regulates ciliary motility in the mucociliary epidermis of Xenopus tadpoles. *Development* **141**, 1526-1533.

Wallmeier, J., Al-Mutairi, D. A., Chen, C.-T., Loges, N. T., Pennekamp, P., Menchen, T., Ma, L., Shamseldin, H. E., Olbrich, H., Dougherty, G. W. et al. (2014). Mutations in CCNO result in congenital mucociliary clearance disorder with reduced generation of multiple motile cilia. *Nat. Genet.* **46**, 646-651.

Werner, M. E. and Mitchell, B. J. (2012). Understanding ciliated epithelia: the power of Xenopus. *Genesis* **50**, 176-185.

Wylie, C. C., Snape, A., Heasman, J. and Smith, J. C. (1987). Vegetal pole cells and commitment to form endoderm in Xenopus laevis. *Dev. Biol.* **119**, 496-502.

DEVELOPMENT

Ying, Q.-L., Nichols, J., Chambers, I. and Smith, A. (2003). BMP induction of Id proteins suppresses differentiation and sustains embryonic stem cell self-renewal in collaboration with STAT3. *Cell* **115**, 281-292.

Yoshizato, K. (2007). Molecular mechanism and evolutional significance of epithelial-mesenchymal interactions in the body- and tail-dependent metamorphic transformation of anuran larval skin. *Int. Rev. Cytol.* **260**, 213-260.

Yu, P. B., Hong, C. C., Sachidanandan, C., Babitt, J. L., Deng, D. Y., Hoyng, S. A., Lin, H. Y., Bloch, K. D. and Peterson, R. T. (2008). Dorsomorphin inhibits BMP signals required for embryogenesis and iron metabolism. *Nat. Chem. Biol.* **4**, 33-41.
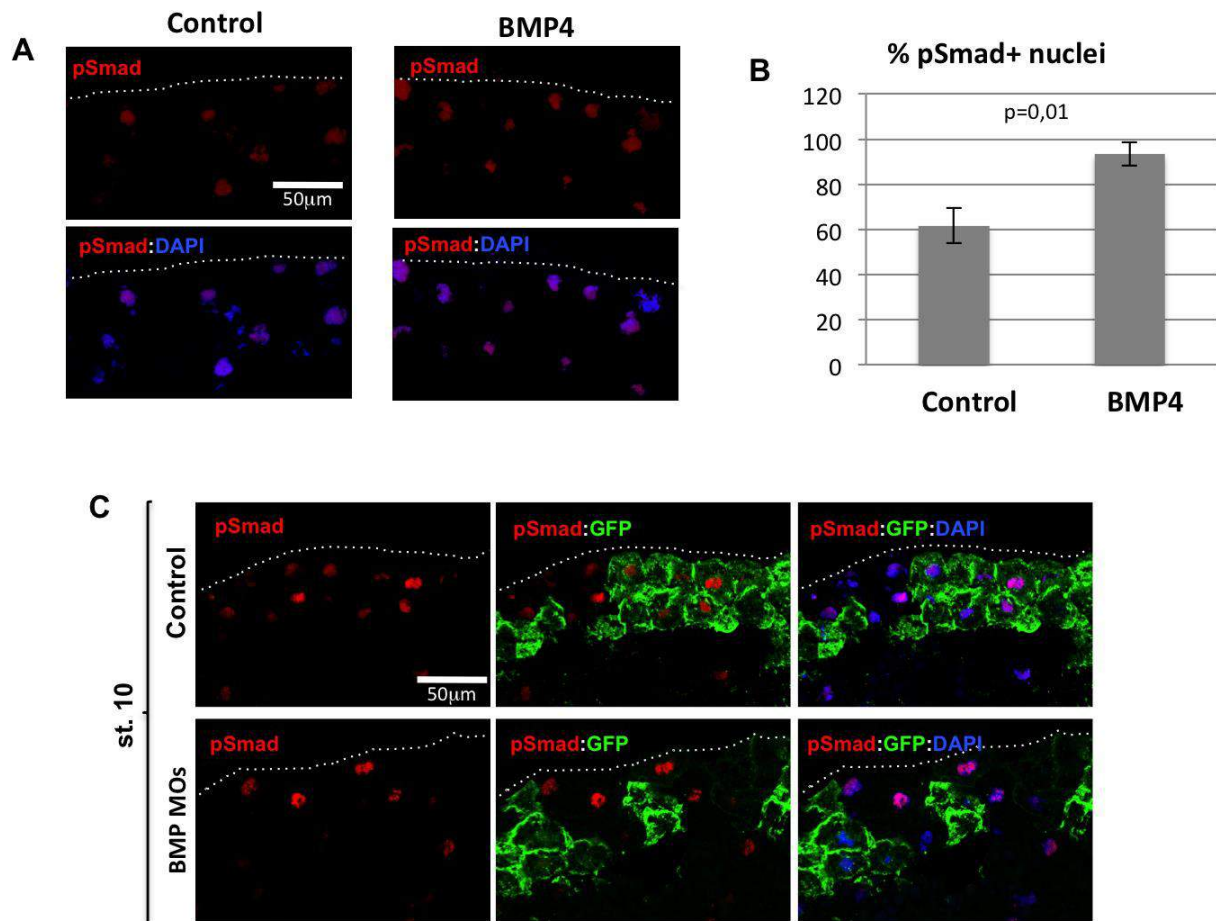
Figure S1: Validation of pSmad1/5/8 staining in response to BMP manipulation.

(**A**): Injection of stage 9 *Xenopus* embryos with recombinant BMP4 led to increased Smad1/5/8 phosphorylation and nuclear localization. (**B**): The percentage of nuclei positive for the pSmad signal is significantly higher in BMP-treated than in control embryos (Student's t-test). (**C**): Knocking down BMP2, BMP4 and BMP7 with specific morpholino oligonucleotides inhibited Smad1/5/8 phosphorylation. Embryos were injected with either GFP mRNA alone (upper row) or GFP mRNA and the BMP2/4/7 MOs (lower row). The pSmad1/5/8 signal was lost in cells that received the BMP2/4/7 MOs, but not in those that received only the GFP mRNA.
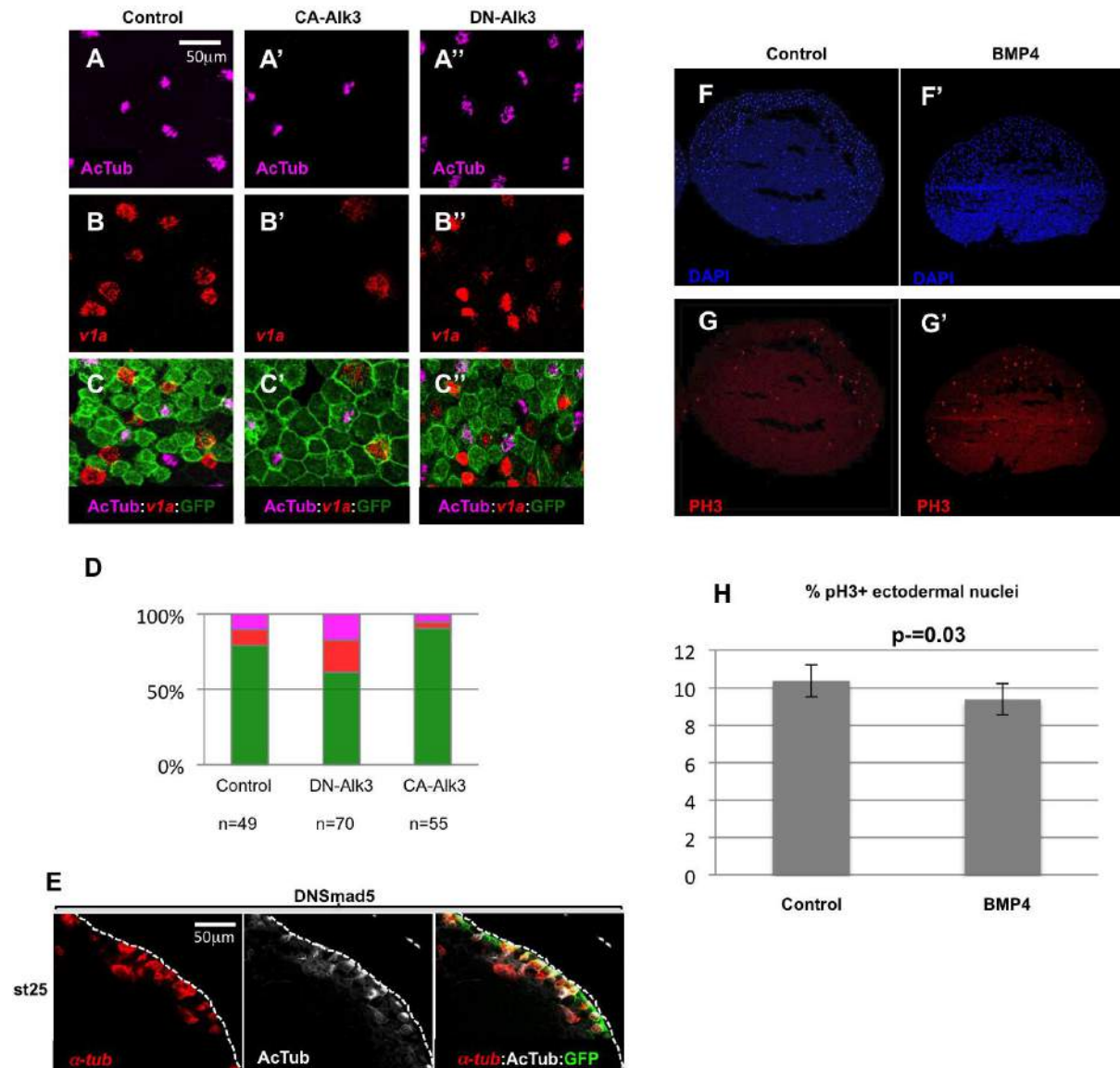
Figure S2: Interfering with the BMP pathway alters the numbers of MCCs and ionocytes in the developing *Xenopus* epidermis.

(A-D): 8-cell stage embryos were injected into the animal ventral blastomeres with synthetic mRNAs coding for GFP, alone (control; A, B, C) or together with mRNAs coding for a constitutively active (CA-Alk3; A', B', C') or a dominant negative (DN-Alk3; A", B", C") version of the BMP receptor ALK3, then hybridized at stage 25 with a probe against the ionocyte marker *v1a* and antibodies against acetylated tubulin and against GFP. Activation of the BMP pathway by CA-Alk3 injection resulted in a decrease in the numbers of MCCs and

ionocytes. Inhibition of the BMP pathway by DN-Alk3 injection results in an increase in the numbers of MCCs and ionocytes. (D): quantification of the different cellular populations in injected epidermal clones. The bars represent the total number of GFP positive cells scored. Magenta: acetylated tubulin positive MCCs; red: *v1a* positive ionocytes; green: GFP positive cells negative for both acetylated tubulin and *v1a*. **(E):** Embryos injected with a synthetic mRNA coding for a dominant negative form of the zebrafish BMP pathway nuclear effector Smad5 (dnSmad5), showed supernumerary *α-tubulin* positive MCC precursors, which only partially managed to intercalate. **(F-H):** Embryos were injected in the blastocoele with BSA (control) or recombinant BMP4 protein (BMP4), fixed at stage 10, cryosectioned and immunostained with an antibody against phosphorylated histone H3 (red), a hallmark of cells in mitosis. DAPI (blue) was used to stain the nuclei. The graph in (H) shows the ratio of phospho-H3 positive nuclei to the total number of ectodermal DAPI stained nuclei. BMP4 injection did not significantly modify the number of mitotic nuclei compared to controls (Student's t-test). In F-G', the animal pole (ectoderm) is up.
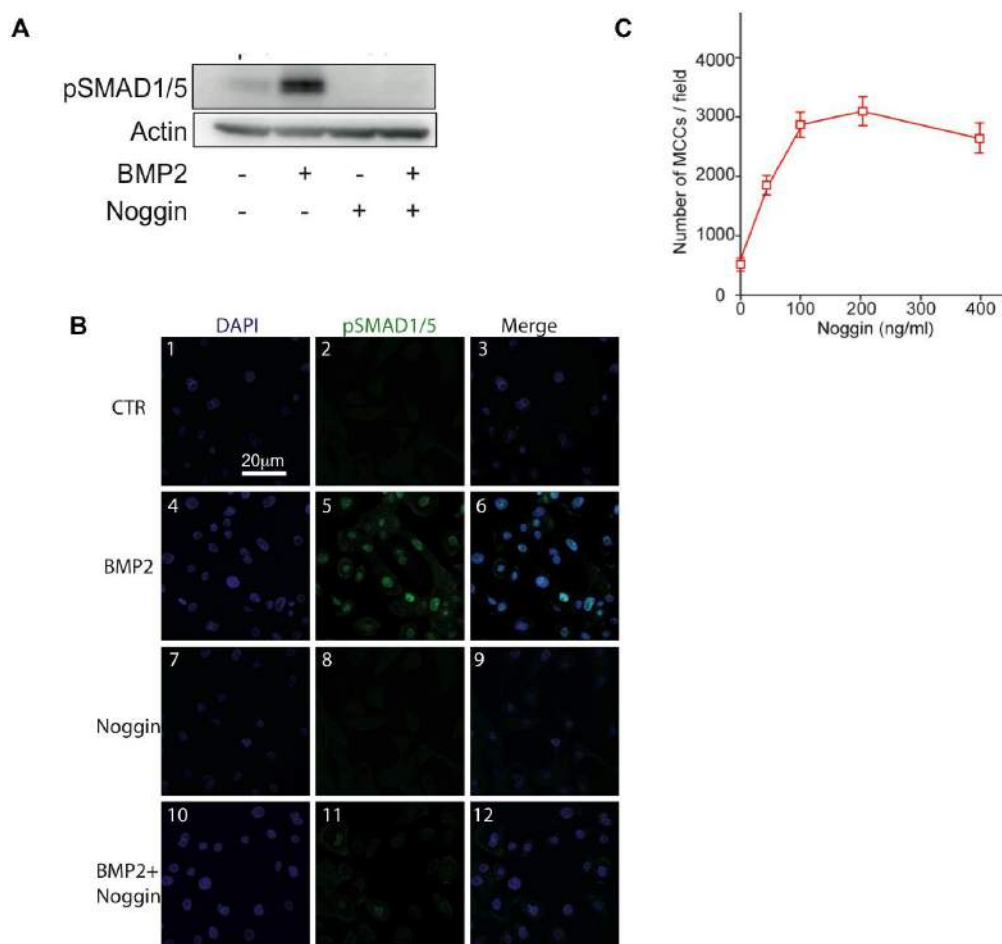
Figure S3: Validation of BMP pathway manipulation in HAECs.

(A): Expression levels of pSMAD1/5 in response to BMP2 (100ng/ml, 2h), Noggin (100ng/ml, 2h), or BMP2+Noggin (100ng/ml each, 2h) in proliferating HAECs. Actin was used as a loading control. **(B)** Proliferating HAECs were stained to identify the specific sub-cellular localization of pSMAD1/5 (in green) in untreated control cells (panels 1-3), BMP2-treated cells (100ng/ml, 2h) (panels 4-6), Noggin-treated cells (100ng/ml, 2h) (panels 7-9) and cells treated with both BMP2 and Noggin (100ng/ml each, 2h) (panels 10-12). Nuclei were stained with DAPI (in blue; panels 1,4,7,10). Data are representative of 3 independent experiments. **(C):** Dose-response curve of Noggin treatment. Regenerating HAECs were chronically treated with different doses of recombinant Noggin. Acetylated-tubulin positive MCCs were counted at LC. 100ng/ml Noggin was the minimal dose to give the maximal effect and used in the rest of the study.
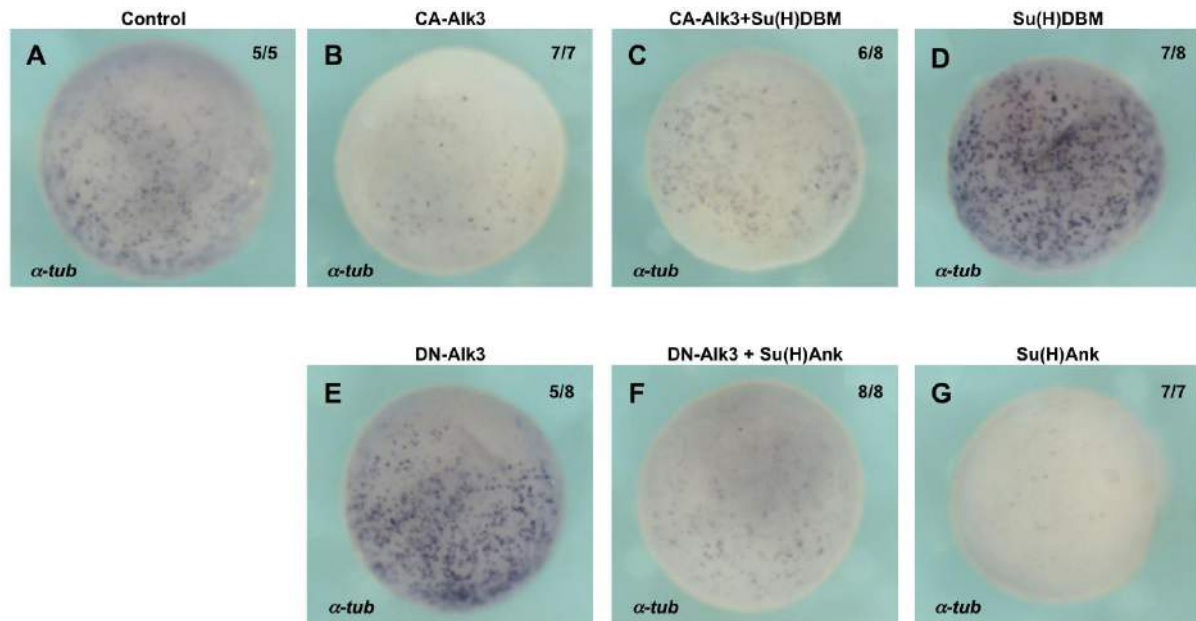
Figure S4: The BMP and Notch pathways interact.

Co-injection of mRNAs coding for a constitutively active form of the BMP receptor Alk3 (CA-Alk3) and a dominant negative form of the transcriptional Notch effector Suppressor-of-hairless (Su(H)DBM) (**C**) mitigated both the loss of α-tubulin positive cells resulting from expression of CA-Alk3 alone (**B**) and their increase following injection of Su(H)DBM alone (**D**). Co-injection of mRNAs coding for a dominant negative form of the BMP receptor Alk3 (DN-Alk3) and a constitutively active form of the transcriptional Notch effector Suppressor-of-hairless (Su(H)Ank) (**F**) mitigated both the increase in α-tubulin positive cells resulting from expression of DN-Alk3 alone (**E**) and their loss following injection of Su(H)Ank alone (**G**). The number of embryos showing the phenotype displayed over the total number of embryos examined is indicated.

Table S1: Plasmids, morpholinos, antibodies, drugs and recombinant proteins used.

Plasmid name	Vector	linearized with	transcribed with
dnSmad5	pCS2+	NotI	SP6
CA-Alk3	pCS2+	NotI	SP6
DN-Alk3	pCS2+	NotI	SP6
GFP-CAAX	pCS105	Ase1	SP6

Morpholino Name	Sequence
MO-BMP2	5'-GATCCCAGCGACCATTGTCAACCTG-3'
MO-BMP4	5'-CAGCATTCGGTTACCAGGAATCATG-3'
MO-BMP7	5'-TTACTGTCAAAGCATTCATTTTGTC-3'

Antibodies used on *Xenopus*	Source	Reference	Dilution
Monoclonal mouse anti-acetylated tubulin	Sigma	Clone 6-11B-1	1:200
Monoclonal mouse 5G7	Gift from Saburo Nagata (Japan Women's University)		1:500
Monoclonal mouse anti-P63	Abcam	Ab111449	1:100
Polyclonal rabbit anti-pSmad1/5/8	Cell signalling	9511	1:100
Polyclonal chicken anti-GFP	2BScientific	GFP-1020	1:1000
Polyclonal rabbit anti-Serotonin	Millipore	Ab938	1/250
Polyclonal rabbit anti-phosphoH3	Millipore	06-570	1 :250
anti-mouse-Cy5 anti-mouse 647 anti-mouse-561 anti-chick-488 anti-rabbit-561	Molecular Probes		1:500

Antibodies used on HAECs	N° clone	Source	Reference	Dilution	
				IF	Blot
Anti-acetylated tubulin	6-11B-1	Sigma-Aldrich	T7451	1 :1000	
Anti-HSP60	K-19	Santa Cruz Biotechnology	sc-1722		1 :5000
Anti-Muc5AC	45M1	Abcam	ab3649	1 :500	
Secondary antibodies		Molecular Probe		1:500	
Anti-pSmad1/5/8	41D10	Cell signaling	9516	1 :100	1 :1000
Anti-Smad1	D59D7	Cell signaling	6944		1 :1000
Anti-Actin	I-19	Santa Cruz Biotechnology	sc-1616		1 :5000

Drug and Recombinant proteins	Source	Reference	Concentration
Dorsomorphin	Sigma-Aldrich	P5499	2mg/ml
BMP2	R&D	355-BM	200ng/ml
Noggin	R&D	6057-NG	200ng/ml or see figures
BMP4	R&D	1128-BM-010	2 to 7ng/embryo

Probe	Vector	linearized	transcribed	Reference
Dll1	pBS	XhoI	T7	Deblandre et al. 1999
FoxA1	pBS	EcoRI	T3	Sinner et al. 2004
FoxJ1	pCS2+	BamHI	T7	Stubbs et al. 2008
Foxi1e	pCMV Sport 6	SalI	T7	Dubaissi et al. 2011
Intelectin-1	pBS	EcoRI	T7	Hayes et al. 2007
Multicilin	pBS	HindIII	T3	Stubbs et al. 2012
Otogelin	pCMV Sport 6	SalI	T7	Hayes et al. 2007
Tph1	pCMV Sport 6	EcoRV	T7	Walentek et al. 2014
α-Tubulin	pBS	NotI	T7	Deblandre et al. 1999
Trim29	pCS2+	EcoRI	T7	Hayes et al. 2007
V1a	pCS107	ClaI	T7	Dubaissi et al. 2011
α-Dystroglycan	pCRII	XhoI	Sp6	Bello et al. 2008

References:

Bello, V. Sirour, C. Moreau, N., Denker, E. and Darribère, T. (2008). A function for dystroglycan in the pronephros development in Xenopus laevis. *Dev. Biol*. **317**,106-120.

Dubaissi, E. and Papalopulu, N. (2011). Embryonic frog epidermis: a model for the study of cell-cell interactions in the development of mucociliary disease. *Dis. Mod. Mech.* **4**, 179-192.

Sinner, D., Rankin, S., Lee, M. and Zorn, A.M. (2004). Sox17 and beta-catenin cooperate to regulate the transcription of endodermal genes. *Development* **131,** 3069-3080.

Stubbs, J.L., Oishi, I., Izpisùa Belmonte, J.C., Kintner, C. (2008). The forkhead protein Foxj1 specifies node-like cilia in Xenopus and zebrafish embryos. *Nat. Genet.* **40**, 1454-1460.